Mathematical Biosciences and Engineering

https://www.aimspress.com/journal/mbe

MBE, 22(11): 2826–2851.
DOI: 10.3934/mbe.2025104
Received: 19 July 2025
Revised: 29 August 2025
Accepted: 09 September 2025
Published: 15 September 2025

Research article

Tumor expansion and immune regulation in a mathematical model of cancer under variations in tumor cell proliferation rate and innate immune stimulation

Manuel Arturo Nova-Martínez[1,*] **and Héctor Andrés Granada-Díaz**[2]

[1] Facultad de Ingeniería, Grupo de Investigación Programas de Ingenierías (Grupo-GIPIS), Universidad Cooperativa de Colombia, Villavicencio 500001, Colombia

[2] Departamento de Matemáticas y Estadística, Grupo de Matemáticas del Tolima (Grupo-MaT), Universidad del Tolima, Ibagué 730001, Colombia

* **Correspondence:** Email: manuel.novam@campusucc.edu.co.

Abstract: In this article, we proposed a simplified mathematical model of primary tumor growth that involves four cell populations: Two types of cancer cells with different levels of immunogenicity, and the immune response in its two components, innate and adaptive. By varying the proliferation rate of non-immunogenic cancer cells and the innate immune stimulation parameter, and applying biparametric numerical continuation techniques, we identified distinct stability regions that revealed scenarios of tumor escape and latency. A closed curve of supercritical Hopf bifurcation points was also detected, delineating the parameter region in which limit cycles emerged. By examining the population maxima of each cell type at steady state, we identified parameter values at which both immunogenic and non-immunogenic tumor cell populations remain in stable equilibrium at modest levels, sustained by an immune response that does not escalate to intensities associated with immunological damage.

Keywords: Hopf bifurcation; immune regulation; limit cycles; mathematical model; non-immunogenic tumors

1. Introduction

When a cancerous tumor emerges, the phenotypic characteristics of tumor cells are not homogeneous [1, 2]; for example, cell morphology, metabolism, angiogenic factors, and antigen expression can vary, and this genetic instability is an obstacle to the immune response. The immunogenicity of a cancer cell refers to its ability to activate the immune response, which depends on the expression of tumor antigens and the release of danger signals that alert the immune system. This is a key factor in the development of immunotherapies for cancer, as non-immunogenic cells

evade immune activation by failing to release the necessary molecules to induce an effective response [3]. In other words, these suppress antigen presentation or modulate their microenvironment to prevent activation.

Research in cancer immunotherapy has established that primary tumors can be recognized and eliminated without external therapeutic intervention [4, 5]. The recognition of malignant cells is mainly due to antigens, in this case, in immunogenic cells; however, due to genetic alterations several variants of tumor cells with low immunogenicity can appear, which in their accumulation become non-immunogenic tumors [6, 7]. The transition from one type to another is a common phenomenon in these biological processes; it also occurs with immune response cells, which can develop conditions that promote tumor growth. For example, the polarization of macrophages between M1 and M2 phenotypes studied in [8] enables that the M1 phenotype produces suppressor molecules while M2 macrophages produce protumoral factors and promote angiogenesis. Similarly, polarization occurs in cytotoxic T cells and natural killer (NK) cells [9, 10].

The characteristics and composition of the tumor microenvironment determine whether a tumor remains immunogenic or becomes non-immunogenic, thereby complicating the effectiveness of therapeutic responses. To investigate tumor growth, experimental investigation has been complemented by mathematical modeling with the aim to quantify and predict these dynamics. Mahlbacher et al. (2019) [11] emphasized the importance of mathematical modeling for understanding the complex interactions between tumor and immune cells, highlighting the diversity of approaches, such as those based on systems of ordinary differential equations. In this context, the literature reports models that capture the essential features of the phenomenon, for example [1, 12–15]. In this work, we study the model presented in [1], which comprises a system of four nonlinear ordinary differential equations. The model incorporates the configuration of the immunogenic tumor phenotype to investigate the effectiveness of the immune system in response to tumor heterogeneity.

Building on this framework, we propose a simplified system in which we conduct a local stability analysis of the equilibrium points and demonstrate the occurrence of a supercritical Hopf bifurcation. Furthermore, we construct a bi-parametric numerical continuation curve of Hopf points and analyze the resulting dynamic scenarios. By simplifying the system, it can be expressed in terms of dimensionless parameter combinations, which facilitates sensitivity analysis since instead of varying many original parameters, and the effect of a few parameters that concentrate the dynamics could be studied. Consequently, the results presented in this work rely on a qualitative mathematical analysis under specific structural and parametric assumptions. These assumptions are intended to highlight the fundamental dynamic mechanisms of the system without aiming to capture the full complexity of the oncological process or to account for all biological variables involved in cancer.

The contents presented in the article are organized as follows: In Section 2, we introduce the model for the evolution of the tumor and derive the dimensionless system. Section 3 is dedicated to the analysis of the local dynamics, where the existence conditions and the stability characteristics for the equilibrium points are studied. Moreover, the emergence of a Hopf bifurcation is demonstrated. In Section 4, bi-parametric numerical continuation techniques are employed to construct a continuation curve of Hopf points, considering variations in the proliferation rate of non-immunogenic cancer cells and the innate immune stimulation parameter. Along this curve, the dynamics of the first Lyapunov coefficient and the transversality condition are analyzed. In Section 5, the population maxima in

steady state are studied; additionally, numerical simulations are presented to illustrate the behavior of the system under the different dynamic scenarios identified, exploring the sensitivity of relevant parameters. Finally, in Section 6, we discuss the results obtained, their biological relevance, and the possible implications of the model for future research.

2. Model description

Alvarez et al. (2019) [1] formulated a tumor cell dynamics model that considers interactions between tumor cells and the immune response, involving four cell populations. We denote the immunogenic tumor population by T_1 and the non-immunogenic tumor cells by T_2. Similarly, E_1 corresponds to the innate immune response effector population, and E_2 represents the adaptive immune response cells. The immunogenic tumor cell population is governed by Eq (2.1).

$$\dot{T}_1 = aT_1(1 - \tfrac{T_1}{k}) - \mu E_1 T_1 - \beta E_2 T_1 - \nu T_1 T_2. \tag{2.1}$$

In Eq (2.1), the first term describes the logistic growth of T_1, limited by the carrying capacity k. The term $-\mu E_1 T_1$ corresponds to the elimination of T_1 mediated by the effector population E_1, which is justified by the direct cytotoxic action of the innate immune response. Similarly, $-\beta E_2 T_1$ reflects the elimination of T_1 induced by E_2, representing the contribution of the adaptive immune response, since, in this context, the E_2 population is recruited in response to the presentation of antigens derived from T_1. Finally, the term $-\nu T_1 T_2$ models the competition between the tumor populations T_1 and T_2 as a simplified representation of competition for space and nutrients.

Eq (2.2) is formulated for T_2 based on the same principles that govern the dynamics of T_1, incorporating the characteristics associated with the non-immunogenic nature of this population and its lower proliferative capacity.

$$\dot{T}_2 = a\rho T_2(1 - \tfrac{T_2}{k}) - \mu q E_1 T_2 - r\nu T_1 T_2. \tag{2.2}$$

In Eq (2.2), the logistic growth of T_2 is constrained by the same carrying capacity k. This assumption is made because both tumor populations proliferate within the same microenvironment and therefore compete for common resources such as nutrients, oxygen, and space. The proliferation rate of T_2 is defined by ap $(0 < p < 1)$. The term $-\mu q E_1 T_2$ represents the elimination of T_2 mediated by the effector population E_1, where parameter q satisfies $0 < q < 1$. Biologically, non-immunogenic tumor cells exhibit immune evasion mechanisms that reduce the effectiveness of the innate response. It is important to note that T_2 is not susceptible to the action of E_2 due to its non-immunogenic nature and the inability of the adaptive immune response to recognize it through antigen presentation. Regarding the competition between tumor populations, the dynamics of T_2 include the term $-r\nu T_1 T_2$, where r is introduced to account for the possibility that the two populations may experience different competitive pressures due to differences in their angiogenic potential, nutrient consumption efficiency, or ability to colonize the available microenvironment.

To model the proliferation of E_1 in response to the tumor, a Michaelis-Menten type mechanism is incorporated, represented by the positive functional defined in Eq (2.3). The parameter s $(0 < s < 1)$ modulates the lower capacity of T_2 cells to induce the innate immune response.

$$\frac{c_4(T_1 + sT_2)E_1}{c_5 + T_1 + T_2}. \tag{2.3}$$

Thus, as shown in Eq (2.4), the dynamics of the innate immune cell population are governed by the balance between activation, proliferation, and elimination processes. Parameter c_1 represents a basal source of cells E_1, while $-c_2E_1$ models their natural death. The recruitment of innate cells is inhibited by the presence of the tumor through the term $-c_3(T_1 + T_2)E_1$.

$$\dot{E}_1 = c_1 - c_2E_1 - c_3(T_1 + T_2)E_1 + \frac{c_4(T_1 + sT_2)E_1}{c_5 + T_1 + T_2}. \tag{2.4}$$

Equation (2.5) is proposed to describe the dynamics of the adaptive immune response cell population. The term $d_1T_1E_1$ represents the activation of E_2, which is directly linked to the activity of the innate population E_1. These cells are responsible for transmitting the activation signal by presenting antigens derived from immunogenic tumor cells T_1. Conversely, the term $-d_2T_1E_2$ models the inhibition of E_2 under an immunogenic tumor burden and represents mechanisms of immune evasion and deactivation of the adaptive response. Finally, the term $-d_3E_2$ represents the natural death of adaptive effector cells.

$$\dot{E}_2 = d_1T_1E_1 - d_2T_1E_2 - d_3E_2. \tag{2.5}$$

Table 1. List of parameters for the model (2.6).

Par.	Description	Units	Value
a	Proliferation rate of T_1 cells	day^{-1}	2.202×10^{-1}
k	Carrying capacity of tumor T_1, T_2 cells	$cell$	2.0×10^{6}
μ	Elimination rate of T_1 cells by E_1	$cell^{-1}day^{-1}$	1.101×10^{-7}
β	Elimination rate of T_1 cells by E_2	$cell^{-1}day^{-1}$	1.101×10^{-7}
ν	Intensity with which T_2 cells affect T_1	$cell^{-1}day^{-1}$	5.15×10^{-8}
c_1	Basal level of the innate immune response E_1	$cell^{-1}day^{-1}$	4.404×10^{-1}
c_2	Death rate of innate immune response cells E_1	day^{-1}	9.909×10^{-2}
c_3	Inactivation rate of E_1 by T_1 and T_2 cells	$cell^{-1}day^{-1}$	3.422×10^{-10}
c_4	Stimulation rate of innate immune cells E_1	day^{-1}	9.909×10^{-1}
c_5	Saturation threshold for immune response	$cell$	2.0×10^{6}
d_1	Activation rate of adaptive cells E_2	$cell^{-1}day^{-1}$	1.1×10^{-7}
d_2	Inactivation rate of E_2 by T_1 cells	$cell^{-1}day^{-1}$	3.42×10^{-10}
d_3	Death rate of adaptative cells E_2	day^{-1}	2.0×10^{-2}
ρ	ρa: proliferation rate of T_2 cells		0.6
q	$q\mu$: elimination rate of T_2 cells by E_1		0.1
r	$r\nu$: intensity with which T_1 cells affect T_2		1.5
s	Relative weight of T_2 in the modulation of E_1		2.222×10^{-3}

Based on the dynamics described in Eqs (2.1)–(2.5), we formulate a system of coupled ordinary differential equations that integrates all interactions among the cell populations. Formally, the dynamics of the four cell populations is given by Eq (2.6), with initial conditions $T_1(0)$, $T_2(0)$, $E_1(0)$, and $E_2(0)$. In the model (2.6), host tissue cells are not represented as an explicit population; their effects are incorporated indirectly through the carrying capacity parameter, k, and the logistic growth

terms. Wilkie and Hahnfeldt (2017) [12] employed this approach in their model, using the carrying capacity as a simplified mechanism to capture the influence of healthy tissue on tumor dynamics, summarizing limitations such as space, nutrient availability, and vascular support.

$$\begin{aligned}
\dot{T}_1 &= aT_1(1-\tfrac{T_1}{k}) - \mu E_1 T_1 - \beta E_2 T_1 - \nu T_1 T_2,\\
\dot{T}_2 &= a\rho T_2(1-\frac{T_2}{k}) - \mu q E_1 T_2 - r\nu T_1 T_2,\\
\dot{E}_1 &= c_1 - c_2 E_1 - c_3(T_1+T_2)E_1 + \frac{c_4(T_1+sT_2)E_1}{c_5+T_1+T_2},\\
\dot{E}_2 &= d_1 T_1 E_1 - d_2 T_1 E_2 - d_3 E_2.
\end{aligned} \tag{2.6}$$

All parameters involved in the model (2.6) are positive values. Table 1 details the physical interpretation of each parameter and a configuration of values taken from [1]. System (2.6) is framed within cancer immunology analysis and differs from the models formulated in [16–18] by not including interactions with host cells, by dividing malignant cells into two groups according to their level of immunogenicity, and by studying separately the dynamics of the innate and adaptive immune responses. Alvarez et al. (2019) [1] described how to obtain the equilibrium points in the model (2.6) and mentioned the emergence of a Hopf bifurcation, which leads to the formation of stable limit cycles. Based on the model (2.6), Kanatnikov and Starkov (2023) [19] applied the method of compact invariant set localization and identified a globally attracting set. They established mathematical conditions under which the tumor evolution converges to the elimination scenario and showed that reducing complexity by eliminating certain variables or restricting the dynamics to invariant subspaces preserves the stability of the equilibria and the conditions for cancer eradication. This suggests that the structure of the system enables a simplified representation without losing the essence of its dynamic behavior.

2.1. Dimensionless model

To simplify the analysis of the system dynamics described by Eq (2.6), it can be reformulated in terms of dimensionless parameter combinations. We assume that the parameters k, a, μ, and β are the constants given in Table 1, and we propose the rescaling described in Eq (2.7), which yields four ODEs for x_1, x_2, x_3, and x_4, representing the dimensionless variables for T_1, T_2, E_1, and E_2, respectively.

$$t' = \frac{t}{a}, \quad T_1 = kx_1, \quad T_2 = kx_2, \quad E_1 = \frac{a}{\mu}x_3, \quad E_2 = \frac{a}{\beta}x_4. \tag{2.7}$$

We substitute the proposed rescaling in Eq (2.7) into system (2.6). After operating appropriately and simplifying, we obtain the following system

$$\begin{aligned}
\dot{x}_1 &= x_1(1-x_1) - x_1x_3 - x_1x_4 - \alpha_1 x_1 x_2,\\
\dot{x}_2 &= \rho x_2(1-x_2) - qx_2x_3 - r\alpha_1 x_1 x_2,\\
\dot{x}_3 &= \alpha_2 - \alpha_3 x_3 - \alpha_4(x_1+x_2)x_3 + \frac{\alpha_5(x_1+s\,x_2)x_3}{\eta+x_1+x_2},\\
\dot{x}_4 &= \rho_1 x_1 x_3 - \rho_2 x_1 x_4 - \rho_3 x_4,
\end{aligned} \tag{2.8}$$

where

$$\alpha_1 = \frac{\nu}{k\,a},\ \alpha_2 = \frac{c_1\,\mu}{a^2},\ \alpha_3 = \frac{c_2}{a},\ \alpha_4 = \frac{c_3}{k\,a},\ \alpha_5 = \frac{c_4}{a},$$
$$\rho_1 = \frac{d_1\beta}{k\,a\,\mu},\ \rho_2 = \frac{d_2}{k\,a},\ \rho_3 = \frac{d_3}{a},\ \eta = c_5\,k. \tag{2.9}$$

The new parameters used in system (2.8) are generated through the equalities of Eq (2.9). After nondimensionalization, the model is expressed in terms of dimensionless parameters representing ratios of comparable quantities; in other words, it represents relationships between rates or timescales than absolute values with units. Since k, a, μ, and β are assumed to be constant, the analysis focuses on the sensitivity of the system to the proliferation rate of non-immunogenic tumor cells and to the parameter of innate immune stimulation, represented by ρ and α_5, respectively. It is worth noting that the simplified model preserves the essential dynamic mechanisms of the original system, namely tumor proliferation, inter population competition, and immune response activation. An important aspect of the dimensionless system described by Eq (2.8) is that it reduces the complexity of the model by concentrating the original biological parameters into a smaller set of combinations. This simplification makes analytical and numerical studies, such as sensitivity and bifurcation analyses, easier because it highlights the parameters that drive the dynamics. From the set of parameters in Table 1 and Eq (2.9), the dimensionless values presented in Table 2 are determined. These values are used to study the evolution of tumor dynamics and its sensitivity to variations in parameters ρ and α_5.

Table 2. Dimensionless parameters for model (2.8).

Parameter	Value	Parameter	Value
ρ	0.6	α_1	4.6776×10^{-1}
q	0.1	α_2	1.0000×10^{-6}
r	1.5	α_4	3.1081×10^{-3}
η	1.0	ρ_1	9.9909×10^{-2}
α_3	0.45	ρ_2	3.1063×10^{-3}
α_5	4.5	ρ_3	9.0827×10^{-2}
		s	2.2222×10^{-3}

3. Local dynamics of tumor growth

3.1. Equilibrium points

We define the vector field $f = [\dot{x}_1, \dot{x}_2, \dot{x}_3, \dot{x}_4]^t$ with $\dot{x}_1, \dot{x}_2, \dot{x}_3, \dot{x}_4$ given by (2.8). The fixed points of f and its stability conditions under variation of the parameters ρ and α_5 are exposed next. To classify each fixed point P of the field f, we use the following convention:

Stability classification: For the equilibrium point P, let $J(P)$ be the jacobian matrix of f at that point. We compute the eigenvalues of the matrix at each point.

- NE: All eigenvalues are real and negative.
- FE: All eigenvalues have negative real components, and there are at least two conjugate complex eigenvalues.

- NS: All eigenvalues are real and nonzero, and at least one of these (but not all) is positive.
- FS: There are at least two complex conjugate eigenvalues, all eigenvalues have nonzero real component, and at least one (but not all) has a positive real part.
- Z: There is an eigenvalue equal to zero, and the others with a nonzero real part.
- H: There are two conjugate complex eigenvalues with zero real part, while the others have negative real component.

3.1.1. Tumor eradication

$P_1 = \left[0, 0, \frac{\alpha_2}{\alpha_3}, 0\right]$ is an equilibrium point of system (2.8) where the tumor cell population becomes extinct, the adaptive immune response is deactivated, and an innate immune response level remains in the microenvironment as a defense mechanism. Constructing the matrix $J(P_1)$ to analyze the local behavior of P_1, we obtain the eigenvalues $\lambda_1 = -\alpha_3$, $\lambda_2 = -\rho_3$, $\lambda_3 = \rho - \frac{\alpha_2}{\alpha_3} q$ and $\lambda_4 = 1 - \frac{\alpha_2}{\alpha_3}$. Based on these eigenvalues, P_1 will be asymptotically stable if $\alpha_2 > \alpha_3$ and $\rho < \frac{\alpha_2}{\alpha_3} q$ hold. With the parameter configuration from Table 2, P_1 is NS with a two-dimensional stable manifold. The stable manifold is defined by the variables x_1 and x_2, meaning convergence to P_1 occurs only under perturbations in x_3 or x_4, in the absence of a tumor. Under these conditions, the elimination scenario will not be feasible in the dynamics of system (2.8). By varying the parameter ρ, we reach the value

$$\rho = \rho_{c_1} = \frac{\alpha_2}{\alpha_3} q = 2.222 \times 10^{-7}, \tag{3.1}$$

where $\lambda_3 = 0$ and P_1 is a point Z.

3.1.2. Interaction between innate immune response and non-immunogenic cells

Subsystem $\mathbf{x_1 = 0}$: Assuming $x_1 = 0$, it is necessarily required that $x_4 = 0$, leading to the subsystem

$$\begin{aligned} \dot{x}_2 &= \rho x_2 (1 - x_2) - q x_2 x_3, \\ \dot{x}_3 &= \alpha_2 - \alpha_3 x_3 - \alpha_4 x_2 x_3 + \frac{\alpha_5 s x_2 x_3}{\eta + x_2}. \end{aligned} \tag{3.2}$$

In system (3.2), there are two feasible equilibrium points ($x_2, x_3 \geq 0$) for the interaction between the non-immunogenic tumor population x_2 and the innate immune response x_3. The first is the projection of P_1, $P_1^* = \left[0, \frac{\alpha_2}{\alpha_3}\right]$, and the second can be expressed as $P_2^* = \left[\hat{x}_2, \frac{p}{q}(1 - \hat{x}_2)\right]$, where $\hat{x}_2$ is a root of the equation of degree three $R_3 x_2^3 + R_2 x_2^2 + R_1 x_2 + R_0 = 0$, such that $0 \leq \hat{x}_2 \leq 1$. The coefficients R_i are determined as a function of the parameters of system (3.2), in particular $R_0 = \eta(\alpha_2 q - \alpha_3 \rho)$. Thus, if condition (3.1) is verified, the root $\hat{x}_2 = 0$ appears and the points P_1^* and P_2^* collide; moreover, P_2^* is feasible for $\rho > \rho_{c_1}$. When crossing the critical value given by Eq (3.1) the equilibrium points P_1^* and P_2^* exchange their stability, leading to a transcritical bifurcation that satisfies the conditions of Sotomayor's theorem [20]. The jacobian matrix of system (3.2) at point P_2^* has the form

$$B = \begin{bmatrix} b_{11} & b_{12} \\ b_{21} & b_{22} \end{bmatrix}, \tag{3.3}$$

so that its eigenvalues are the solutions of the equation

$$\lambda^2 - Tr(B)\lambda + Det(B) = 0. \tag{3.4}$$

In the trace vs determinant diagram shown in Figure 1, for $\rho \in (\rho_{c_1}, 1)$ and $\alpha_5 \in (0, 9)$, the stability characteristics of equilibrium P_2^* are distinguished. Specifically, under the variation of these parameters, Eq (3.4) always has two real negative solutions. Furthermore, in the phase plane of system (3.2) (see Figure 1), which was constructed using the parameters from Table 2 with $\rho = 0.63$ and $\alpha_5 = 0.5$, asymptotic convergence to the equilibrium point $P_2^* = [0, 1]$ is observed. This scenario shows tumor escape within this subsystem.

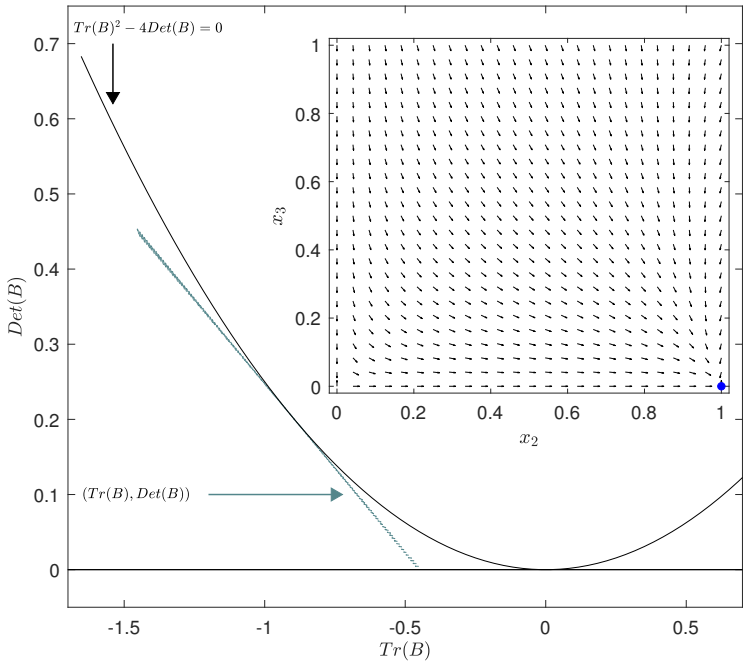

Figure 1. Trace vs Determinant diagram with matrix B defined in Eq (3.3), for the dynamics of point P_2^* in subsystem (3.2), with $\rho \in (\rho_{c_1}, 1)$, $\alpha_5 \in (0, 9)$, and the other parameters fixed at the values in Table 2. Internally, the phase plane x_2, x_3 is shown for the values $\rho = 0.63$ and $\alpha_5 = 0.5$.

Complete system: The dynamics summarized in Figure 1 correspond to subsystem (3.2); however, if we consider system (2.8), $P_2 = \left[0, \hat{x}_2, \frac{p}{q}(1 - \hat{x}_2), 0\right]$, and the jacobian matrix

$$J(P_2) = \begin{bmatrix} a_{11} & 0 & 0 & 0 \\ a_{21} & b_{11} & b_{12} & 0 \\ a_{31} & b_{21} & b_{22} & 0 \\ a_{41} & 0 & 0 & a_{44} \end{bmatrix},$$

whose eigenvalues are

$$\lambda_1 = 1 - \frac{p}{q} + \left(\frac{p}{q} - \alpha_1\right)\hat{x}_2, \qquad \lambda_2 = -\rho_3,$$

and $\lambda_{3,4}$ the solutions of Eq (3.4). $\lambda_1 > 0$ when $\rho \in (\rho_{c_1}, 1)$ and $\alpha_5 \in (0, 9)$, therefore P_2 is NS. With these characteristics, point P_2 has a three-dimensional stable manifold and, due to the presence of a

positive eigenvalue, a one-dimensional unstable manifold. In this sense, if the initial condition lies within the stable manifold, the trajectory will converge to equilibrium as shown in the phase plane in Figure 1. However, any perturbation of the initial condition along the unstable manifold direction will cause the system trajectory to diverge from equilibrium, revealing a drastic change in the dynamics. The transcritical bifurcation in subsystem $x_1 = 0$ is not valid in the complete model (2.8) because, although the collision between the equilibrium points P_1 and P_2 occurs, there is no evidence of an exchange of stability, and only the dimension of the stable manifold is modified.

3.1.3. Interaction between immunogenic cells and immune response

Subsystem $\mathbf{x_2 = 0}$: If $x_2 = 0$, we obtain the subsystem

$$\begin{aligned} \dot{x}_1 &= x_1(1 - x_1) - x_1x_3 - x_1x_4, \\ \dot{x}_3 &= \alpha_2 - \alpha_3x_3 - \alpha_4x_1x_3 + \frac{\alpha_5x_1x_3}{\eta + x_1}, \\ \dot{x}_4 &= \rho_1x_1x_3 - \rho_2x_1x_4 - \rho_3x_4. \end{aligned} \tag{3.5}$$

By calculating the equilibrium points of system (3.5), we obtain $P_1^{**} = \left[0, \frac{\alpha_2}{\alpha_3}, 0\right]$ and $P_3^* = [\hat{x}_1, \hat{x}_3, \hat{x}_4]$ with

$$\hat{x}_3 = \frac{\alpha_2}{\alpha_3 + \alpha_4\hat{x}_1 - \frac{\alpha_5\hat{x}_1}{\eta+\hat{x}_1}}, \quad \hat{x}_4 = \frac{\rho_1\hat{x}_1\hat{x}_3}{\rho_3 + \rho_2\hat{x}_1},$$

where $\hat{x}_1$ is one of the solutions of the degree four equation

$$S_4x_1^4 + S_3x_1^3 + S_2x_1^2 + S_1x_1 + S_0 = 0. \tag{3.6}$$

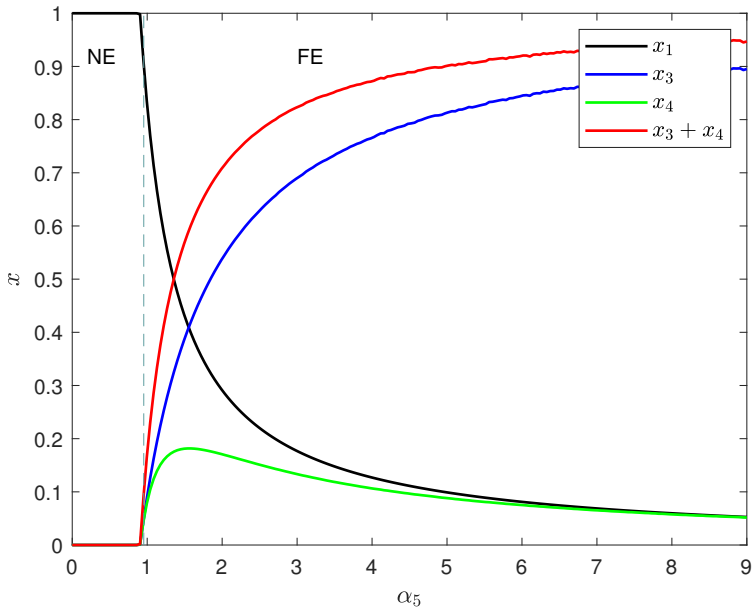

Figure 2. Steady state population dynamics of system (2.8) as a function of parameter a_5 under the condition $x_2 = 0$.

The coefficients S_i in Eq (3.6) are defined as a function of the system parameters (3.5), in particular the term $S_0 = \eta\rho_3(\alpha_3 - \alpha_2)$. Note that the equations of system (3.5) are independent of ρ, so their stability is as well. According to the fundamental theorem of algebra, Eq (3.6) has up to four roots, but for P_3^* to be feasible it must be verified that $0 \leq x_1 \leq 1$. By varying the parameter $\alpha_5 \in (0, 9)$, and the other parameters fixed at the values in Table 2, only one root satisfies the required condition. Then, the equilibrium P_3^* always exists in the parameter configurations analyzed, and there are no collisions of this equilibrium with other equilibria; nevertheless, its stability properties vary. Figure 2 shows that although P_3 is always stable for $\alpha_5 \in (0, 9)$, there exists a critical value $\alpha_5 = \alpha_{5_c} = 0.97412$ at which it changes from NE to a FE. This figure shows an intersection point between the population densities of the immunogenic tumor and innate effector cells ($x_1 = x_3 \approxeq 0.41$), where a maximum in the density of the adaptive immune response is also generated. It should be noted that from this point on, in steady state, the cancer cell population decreases, being controlled by an immune response that does not reach high values. As shown in the figure, when the adaptive immune response remains below 0.1, the tumor population can be controlled over time, stabilizing at low levels.

Complete system: For system (2.8) $P_3 = [\hat{x}_1, 0, \hat{x}_3, \hat{x}_4]$, and the jacobian matrix

$$J(P_3) = \begin{bmatrix} J_{11} & J_{12} & J_{13} & J_{14} \\ 0 & J_{22} & 0 & 0 \\ J_{31} & J_{32} & J_{33} & 0 \\ J_{41} & 0 & J_{43} & J_{44} \end{bmatrix}.$$

If we compute the eigenvalues of the matrix $J(P_3)$, we get

$$\lambda_2 = \rho - q\hat{x}_3 - r\alpha_1\hat{x}_1, \tag{3.7}$$

and the eigenvalues $\lambda_{1,3,4}$, which are solutions of the characteristic equation $\lambda^3 + L_1\lambda^2 + L_2\lambda^2 + L_3 = 0$, where $L_1 = -\mathrm{Tr}(C)$, $L_2 = \frac{1}{2}[\mathrm{Tr}^2(C) - \mathrm{Tr}(C^2)]$, and $L_3 = -\det(C)$, with C being the submatrix

$$C = \begin{bmatrix} J_{11} & J_{13} & J_{14} \\ J_{31} & J_{33} & 0 \\ J_{41} & J_{43} & J_{44} \end{bmatrix}.$$

In the subsystem, $x_2 = 0$, which yields the matrix C, so an equilibrium point is obtained. This point is an attractor (NE or FE) as shown in Figure 2. Now, in the complete model (2.8), the local stability properties of point P_3, using the parameters from Table 2 while varying $\rho \in (\rho_{c_1}, 1)$ and $\alpha_5 \in (0, 9)$, fully agree with the results of stability presented in Figure 2. This agreement arises because in $J(P_3)$, the eigenvalue associated with the x_2 direction, λ_2 given by (3.7), remains consistently negative in the region of interest. In this context, the scenario where P_3 is stable may be relevant, as the eradication of non-immunogenic cells x_2 combined with the interaction of the immune response with immunogenic cells x_1 could represent a desirable state in terms of tumor dynamics. When analyzing the steady state, the population dynamics depend on the value of α_5 as illustrated by the curves drawn in Figure 2. In the region where P_3 is NE ($\alpha_5 \in (0, \alpha_{5_c})$), the level of immunogenic cells approaches its maximum capacity, leading to a tumor escape state, which is an unfavorable scenario for tumor control. This

behavior is also evident in the temporal evolution (see Figure 8(a)). On the other hand, when P_3 is FE and α_5 takes higher values, the level of x_1 cells remains low, but the threshold of the innate immune response increases significantly (see Figure 2 and Figure 8(b)).

3.1.4. Nontrivial coexistence

The nontrivial equilibrium points of model (2.8) are obtained by solving the system

$$1 - x_1 - x_3 - x_4 - \alpha_1 x_2 = 0, \tag{3.8}$$

$$\rho(1 - x_2) - q x_3 - r\alpha_1 x_1 = 0, \tag{3.9}$$

$$\alpha_2 - \alpha_3 x_3 - \alpha_4 (x_1 + x_2) x_3 + \frac{\alpha_5 (x_1 + s x_2) x_3}{\eta + x_1 + x_2} = 0, \tag{3.10}$$

$$\rho_1 x_1 x_3 - \rho_2 x_1 x_4 - \rho_3 x_4 = 0. \tag{3.11}$$

From Eq (3.11), it will be obtained that $x_4 = \frac{\rho_1 x_1 x_3}{\rho_3 + \rho_2 x_1}$. Solving Eq (3.9) in x_2 and substituting in (3.8) gives the following results

$$1 - \left(1 + \frac{r\alpha_1^2}{q}\right) x_1 - (1 + \alpha_1 \rho)\, x_3 - \frac{\rho_1 x_1 x_3}{\rho_3 + \rho_2 x_1} = 0,$$

from which

$$x_3 = \frac{1 - \left(1 + \dfrac{r\alpha_1^2}{q}\right) x_1}{1 + \alpha_1 \rho + \dfrac{\rho_1 x_1}{\rho_3 + \rho_2 x_1}}.$$

The obtained expressions are substituted into Eq (3.10) generating an equation of sixth degree in the variable x_1, whose coefficients are defined in terms of model (2.8) parameters. These coefficients have an extensive and complex form, so it is decided not to write them here; however, in the light of the fundamental theorem of algebra, it can be guaranteed that the maximum number of equilibrium points is six. With the parameter configuration from Table 2, there will be a single feasible nontrivial equilibrium point $P_4 = (\bar{x}_1, \bar{x}_2, \bar{x}_3, \bar{x}_4)$ ($\bar{x}_i > 0, i = 1, 2, 3, 4$). By varying the parameters $\rho \in (\rho_{c_1}, 1)$ and $\alpha_5 \in (0, 9)$, the existence and stability conditions of P_4 have been studied numerically as summarized in Table 3 and Figure 3. These results indicate that P_4 is feasible in regions R9 (FE), R10 (H), R12 (FE), and R13 (FS). Conditions where P_4 is feasible and stable are of great interest, as it represents a coexistence scenario between immunogenic cells x_1, non-immunogenic cells x_2, and the innate x_3 and adaptive x_4 immune responses, where all involved populations persist at constant levels over time. In the context of tumor dynamics, the stability of P_4 is interpreted as a state in which the immune system ensures partial tumor control, maintaining the number of cancer cells at a fixed level. This is observed in clinical situations, such as tumors that remain in latent phases or under immune surveillance, where the presence of cancer is contained without significant progression.

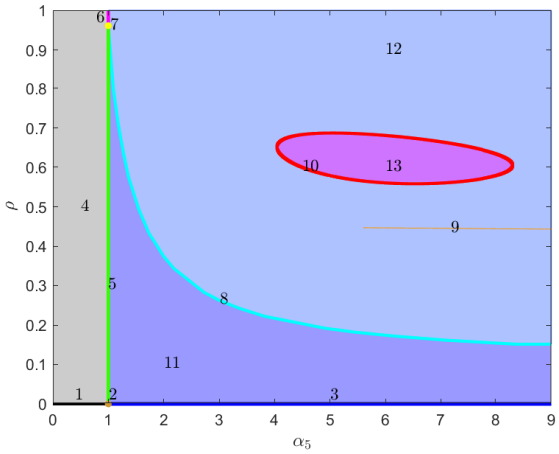

Figure 3. Tumor dynamics for system (2.8) summarized in 13 regions (R1–R13) with $\rho \in (\rho_{c_1}, 1)$, $\alpha_5 \in (0, 9)$, and the other parameters fixed at the values in Table 2. It is constructed by performing a numerical continuation of the eigenvalues of the jacobian matrix of system (2.8) at the equilibrium points P_1, P_2, P_3 and P_4, over the region of parameters under study, and applying the stability classification described above.

Table 3. Tumor dynamics for system (2.8) summarized in 13 regions (R1–R13) with $\rho \in (\rho_{c_1}, 1)$, $\alpha_5 \in (0, 9)$, and the other parameters fixed at the values in Table 2. We use the symbol $\rightarrow$ to indicate a qualitative change in stability. Regions R1–R13 correspond to those outlined in Figure 3.

Region	Feasible equilibrium	Stability
R1	P_1, P_3	Z, NE
R2	P_1, P_3	$Z, NE^{R1} \rightarrow FE^{R3}$
R3	P_1, P_3	Z, FE
R4	P_1, P_2, P_3	NS, NS, NE
R5	P_1, P_2, P_3	$NS, NS, NE^{R4} \rightarrow FE^{R11}$
R6	P_1, P_2, P_3	$NS, NS, NE^{R4} \rightarrow FI^{R12}$
R7	P_1, P_2, P_3	$NS, NS, NE^{R4} \rightarrow FI^{R12}$
R8	P_1, P_2, P_3	$NS, NS, NE^{R11} \rightarrow FI^{R12}$
R9	P_1, P_2, P_3, P_4	NS, FS, FI, FE
R10	P_1, P_2, P_3, P_4	NS, NS, FI, H
R11	P_1, P_2, P_3	NS, NS, FE
R12	P_1, P_2, P_3, P_4	NS, NS, FI, FE
R13	P_1, P_2, P_3, P_4	NS, NS, FI, FI

Table 3 and Figure 3 summarize the characterization of existence and stability conditions of the feasible equilibrium points of system (2.8) under the variation of parameters ρ and α_5. In regions R1–R3, where $\rho = \rho_{c_1}$, equilibrium points P_1 and P_3 are feasible; P_1 is a Z point, and the stability of P_3 depends on the critical value $\alpha_5 = \alpha_{5_c}$ transitioning from NE in R1 to FE in R3. For $\alpha_5 < \alpha_{5_c}$ and $\rho > \rho_{c_1}$, region R4 (see Figure 3) consists of three equilibrium points: P_1, P_2 (NS) and P_3 (NE). The convergence of the trajectories to P_3 in R4 implies that the immunogenic cancer cells x_1 reach their maximum capacity, while the populations x_2, x_3 and x_4 become extinct. This result shows the tumor progression and the escape scenario (see Figure 7 and Figure 8(a)). As observed in Table 3 and Figure 3, regions R4, R5, and R11 contain three feasible equilibrium points: Two of type NS (P_1, P_2) and P_3, which changes stability at the critical value α_{5_c} transitioning from NE in R4 to FE in R11. Region R6 is defined by the parameter values $\alpha_5 = \alpha_{5_c}$ and $\rho > \rho_{c_2} = 0.96118$. In regions R4, R6, and R12, the number of equilibrium points varies with the critical value α_{5_c}, since at $\alpha_5 = \alpha_{5_c}$ the nontrivial equilibrium point P_4 emerges with an FE structure. These regions contain P_1 and P_2 (NS), while equilibrium point P_3 transitions from NE in R4 to FS in R12 (whenever $x_1 \neq 0$ and $x_2 \neq 0$). Region R7 is characterized by $\alpha_5 = \alpha_{5_c}$ and $\rho = \rho_{c_2}$, where R4, R5, R6, R8, R11, and R12 intersect.

According to Table 3 and Figure 3, region R8 marks the boundary between regions R12 and R11, and beyond this threshold, the nontrivial equilibrium point P_4 becomes feasible. Within R12, in addition to P_4 (FE), the equilibrium points P_1, P_2 (NS), and P_3 (FS) also exist. In this region, the system trajectories converge to the nontrivial equilibrium where all interacting populations remain at constant levels in the steady state. Conversely, in region R13, the equilibrium points P_1, P_2 (NS), P_3 (FS), and P_4 (FS) are present. Consequently, in R13, the trajectory of the system does not converge to an equilibrium point, but instead evolves toward a limit cycle, as will be demonstrated in Section 4. In region R11, three trivial equilibrium points are guaranteed, P_1, P_2 (NS), and P_3 (FE). Moreover, there are four equilibrium points in region R9: P_1 (NS), P_2, P_3 (FS), and P_4 (FE). The points that define the curve R10 correspond to Hopf bifurcation points at P_4, this will be demonstrated in Section 4. Table 3 and Figure 3 provide a comprehensive summary of the local dynamics and define the robustness map of system (2.8). Each region in Figure 3 corresponds to a unique stable equilibrium point, with the exception of $R13$, where no stable equilibria are present. Thus, for any initial condition, the system trajectories converge asymptotically to the associated stable equilibrium point or, in the case of $R13$, to a limit cycle.

3.2. Periodic tumor dynamics and immune regulation

By varying the parameters ρ and α_5, a transition in the equilibrium states is observed around the equilibrium point P_4, from the region R12 to the region R13 (see Table 3 and Figure 3). To calculate the eigenvalues of the matrix $J(P_4)$, we obtain the characteristic equation

$$\lambda^4 + L_1\lambda^3 + L_2\lambda^2 + L_3\lambda + L_4 = 0, \tag{3.12}$$

where the coefficients L_i are defined directly by the matrix $J(P_4)$. A Hopf bifurcation occurs when the solutions of (3.12) are two nonzero real numbers and two pure imaginary roots defined of the form $\lambda_1 = \omega\, i$, $\lambda_2 = -\omega\, i$, with $\omega > 0$. Assuming the existence of such solutions and substituting λ_1 or λ_2 into Eq (3.12), we must ensure that both the real and imaginary parts vanish. Then, the conditions for

the existence of a Hopf bifurcation in system (2.8) are derived; these are presented below.

$$L_1^2 - L_1 L_2 L_3 + L_1^2 L_4 = 0, \quad \omega^2 = \frac{L_3}{L_1} > 0.$$

With the parameter configuration given in Table 2, it is obtained the equilibrium point $P_4 = [0.18980, 0.71220, 0.39511, 0.08196]$. By varying the parameter α_1 we reach the critical value $\alpha_{1_0} = 0.72921$ where a point H appears, whose coordinates are $P_{4H} = [0.17971, 0.62123, 0.30698, 0.06031]$. There the eigenvalues for the jacobian matrix $J(P_4)$ are

$$\begin{aligned} \lambda_1 &= 0.31068\, i, & \lambda_2 &= -0.31068\, i, \\ \lambda_3 &= -0.10472, & \lambda_4 &= -0.53913, \end{aligned}$$

then, two pure imaginary eigenvalues and two negative real ones. The numerical continuation of the equilibrium point P_4 under the variation of α_1 and the behavior of the real and imaginary components of the eigenvalues in the neighborhood of the point P_{4H} are shown in Figure 4. The emergence of point H at α_{1_0} is observed, along with a positive transversality condition.

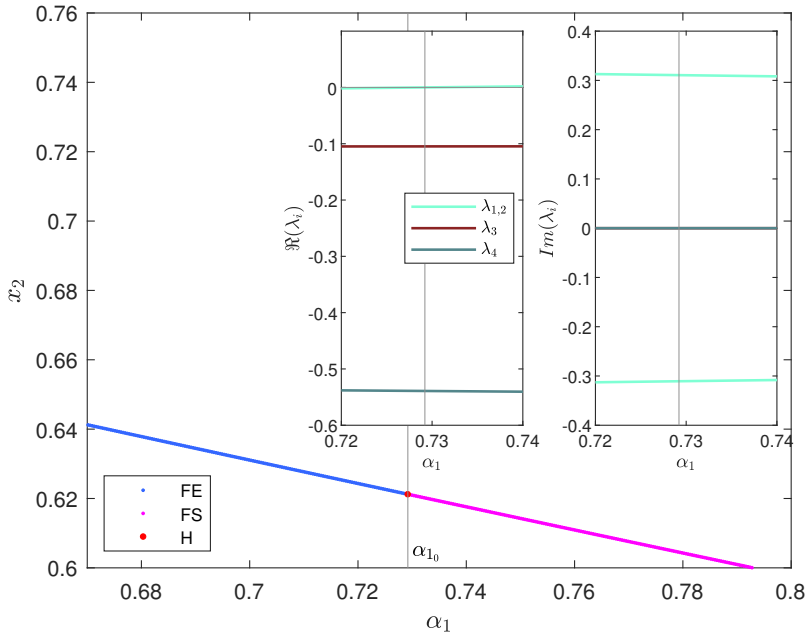

Figure 4. Numerical continuation of equilibrium point P_4 with respect to α_1, with parameters from Table 2. Stability classification and verification of the Hopf transversality condition are shown.

Numerically, for a Hopf bifurcation parameter μ with a critical value μ_0, the transversality condition can be obtained using the discretization

$$d = \frac{\Re(\lambda(\mu_0 + \Delta)) - \Re(\lambda(\mu_0 - \Delta))}{2\,\Delta}, \tag{3.13}$$

with $\Delta = 0.01$ and λ as an eigenvalue associated with the bifurcation. We use (3.13) with $\mu_0 = \alpha_{1_0}$, and $d = 0.17468$ is obtained, which satisfies the requirement for the existence of a Hopf bifurcation.

By employing the Matcont software [21], the first Lyapunov coefficient (see [22]) is computed as $l_1 = -6.393036 \times 10^{-2} < 0$. The numerical results shown for the existence of a purely imaginary eigenvalue pair and the transversality condition are the requirements for the existence of a Hopf bifurcation, according to Hopf's theorem [23]. Then, we have the proof of the following theorem.

Theorem 1. *In system* (2.8)*, a supercritical Hopf bifurcation occurs above the nontrivial equilibrium point P_4 when parameter α_1 crosses the critical value α_{1_0}.*

Figure 4 shows that the equilibrium point P_4 loses stability at the critical value α_{1_0}. According to Theorem 1, a stable limit cycle then emerges, representing oscillatory dynamics among the four cellular populations. This behavior illustrates scenarios in which the immune response fails to sustain continuous control over tumor growth, leading to alternating phases of expansion and immune regulation.

4. Bi-parametric continuation of the Hopf bifurcation

Theorem 1 guarantees the existence of a Hopf bifurcation in system (2.8), and enables us to identify the point P_{4H}, which is a nontrivial equilibrium. In particular, this point is obtained for $\rho = 0.6$ and $\alpha_5 = 4.5$. Since P_4 depends continuously on parameters ρ and α_5, and the eigenvalues of the matrix $J(P_4)$ also vary continuously with respect to these parameters, it is possible to analyze their evolution. In this context, by varying the values of ρ and α_5, and considering the continuity of system (2.8), it is possible to determine configurations that lead to points H. As a bi-parametric continuation methodology, Algorithm 1 is implemented, and the result obtained is the closed curve R10 plotted in Figure 3.

Algorithm 1. *Continuation curve of H points in codimension two.*

1) *The parameters of system* (2.8) *assume the values from Table 2, except for ρ, which is taken in the interval* $(0.55, 0.7)$*, and α_5, which varies in the interval* $(4, 8.3)$*.*
2) *The interval for each parameter is partitioned into 2000 equidistant points, and the cartesian product* $(4, 8.3) \times (0.55, 0.7)$ *is considered.*
3) *For each pair (α_{5_i}, ρ_i) from the cartesian product constructed in step 2, the equilibrium point P_4 is computed, along with the jacobian matrix $J(P_4)$ and its eigenvalues.*
4) *Using a tolerance of 1×10^{-6}, pairs (α_5, ρ) are selected where the matrix $J(P_4)$ has two purely imaginary eigenvalues, $\lambda_1 = \omega\, i$, $\lambda_2 = -\omega\, i$, with $\omega > 0$.*
5) *The pairs (α_5, ρ) obtained in step 4 are drawn in the plane $\alpha_5\rho$.*

Through Algorithm 1, we examine the region of parameters where point P_4 is feasible (violet region of the Figure 3), identifying pairs of values (α_5, ρ), where P_4 is point H. In this sense, the points of the curve R10 (see Figure 3) are H points and delimit the region R13 in which periodic orbits emerge. Within R13, the system does not converge to an equilibrium point but instead evolves oscillatory, reflecting a recurrent interaction between tumor growth and the immune response. To analyze the dynamics of the first Lyapunov coefficient l_1 at the points of curve R10, the Matcont software [21] is used. For this, once point P_{4H} is identified, the numerical continuation of H points in codimension two is carried out, thus obtaining coefficient l_1, corresponding to each point of the curve.

As shown in Figure 5, coefficient l_1 takes negative values at each H point on the R10 curve. This indicates that the curve is associated with a supercritical Hopf bifurcation, regardless of the configuration selected (α_5, ρ). In addition to the first Lyapunov coefficient, the dynamics of the transversality condition at the Hopf bifurcation points is examined. For this, considering $\lambda(\alpha_5)$ as an eigenvalue of the matrix $J(P_4)$, such that $\Re(\lambda(\alpha_{5H})) = 0$, the derivative

$$d_1 = \frac{\partial}{\partial \alpha_5} \Re(\lambda(\alpha_5))\Big|_{\alpha_5=\alpha_{5H}},$$

is computed numerically using the discretization given by Eq (3.13) with $\mu_0 = \alpha_{5H}$. In the same sense, for the variation of parameter ρ

$$d_2 = \frac{\partial}{\partial \rho} \Re(\lambda(\rho))\Big|_{\rho=\rho_H}.$$

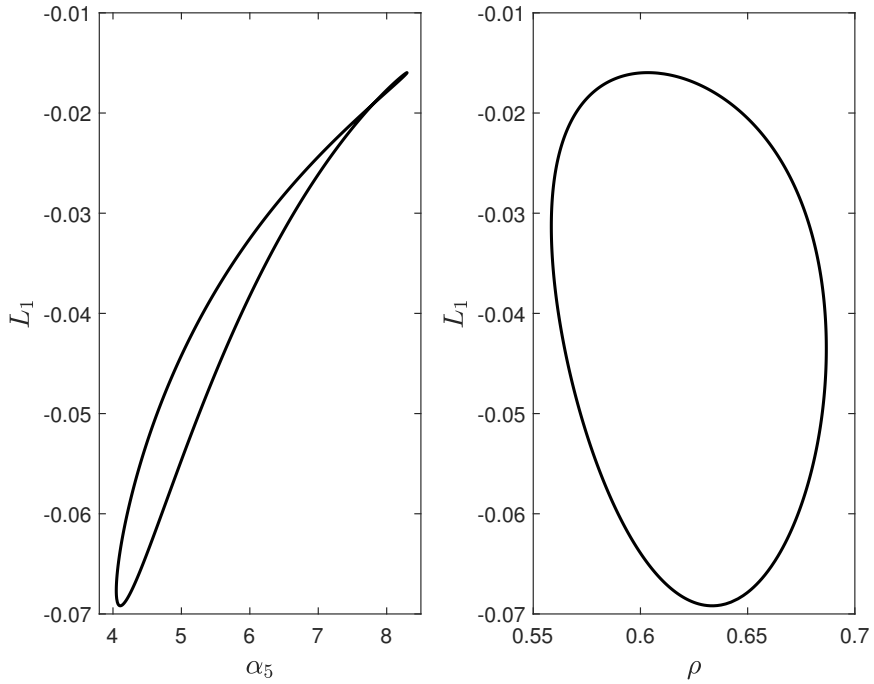

Figure 5. Dynamics of the first Lyapunov coefficient l_1 for the Hopf bifurcation at the H points of curve R10 defined in Figure 3.

As an example, the values for d_1 and d_2 are presented for the representative points highlighted in Figure 6. For the red point, with $\rho_H = 0.63$ and $\alpha_{5H} = 4.126497$, $d_1 = 0.01018$ is obtained. For the green point, where $\rho_H = 0.63$ and $\alpha_{5H} = 8.08535$, $d_1 = -0.00628$ was found. Similarly, at the yellow point, with $\rho_H = 0.56245$ and $\alpha_{5H} = 5.8$, $d_2 = 3.19579 \times 10^{-4}$ was obtained; while with $\rho_H = 0.68288$ and $\alpha_{5H} = 5.8$ (cyan point), the resulting value is $d_2 = -1.90284 \times 10^{-4}$. These derivatives can be calculated for any point on the R10 curve which allows verification of the transversality in each particular configuration (α_5, ρ). Although in region R13, the real component of the eigenvalue λ is close to zero, on a scale of 1×10^{-3}, as observed in Figure 6, a nonzero crossing speed is evident. The analysis of the dynamics of the transversality condition and the first Lyapunov coefficient developed in

this section ensures that supercritical Hopf bifurcations occur along curve R10. As a consequence, the emergence of stable periodic orbits in region R13 is guaranteed.

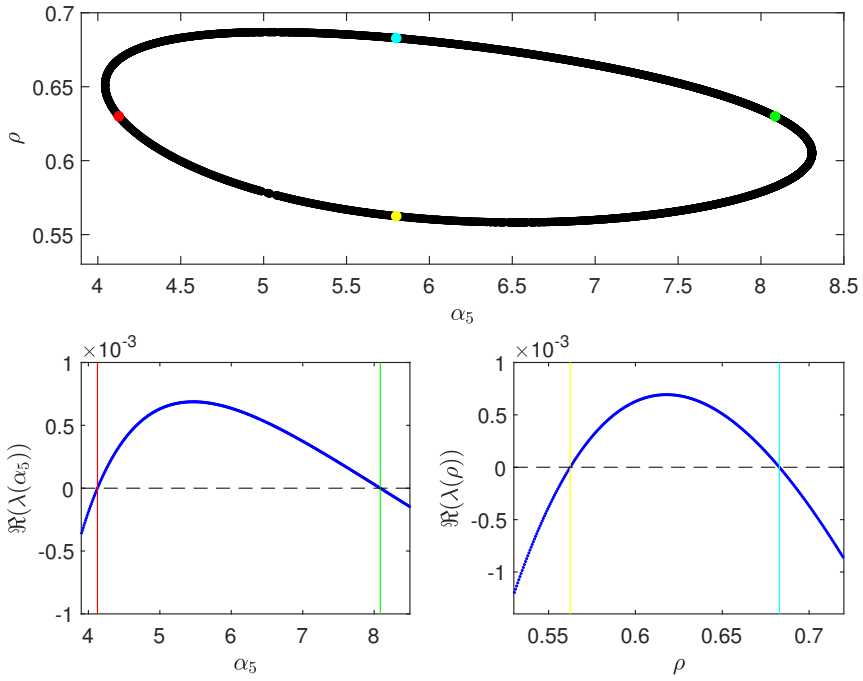

Figure 6. Dynamics for the transversality condition at four representative points. Top: Curve R10. Bottom left: Trajectory of the real component of eigenvalues for $\rho = 0.63$ and varying α_5. Lower right: Trajectory of the real component of eigenvalues for $\alpha_5 = 5.8$ and varying ρ. The other parameters in Table 2 must be taken into account as well.

5. Numerical simulations of tumor evolution

In this section, we analyze the evolution of cell populations and the interaction between the tumor and the immune response, examining the dynamic scenarios described in Table 3 and Figure 3, from states of escape equilibrium or tumor dormancy to periodic behaviors associated with Hopf bifurcation. We show how the dynamic behavior of model (2.8) depends on the rate of proliferation of non-immunogenic cells and the rate of stimulation of the innate immune response.

5.1. Population maxima

Section 3.1.2 showed that in the parameter domain under investigation, the condition $x_1 = 0$ implies convergence to a tumor escape equilibrium, namely the point $P_2 = [0, 1, 0, 0]$. Similarly, the condition $x_2 = 0$ leads to convergence toward the equilibrium point P_3, which may display either an NE or an FE structure as summarized in Figure 2. On the other hand, for initial conditions $x_i > 0,\ i = 1, 2, 3,$ and 4, Figure 3, with the summary in Table 3, indicate the convergence of trajectories as a function of the parameter pairs (α_5, ρ) under analysis; moreover, system (2.8) does not exhibit bistability scenarios, as explained in Section 3.1.4. The only possible variation, depending on the initial conditions and

integration time, arises in region $R13$, where periodic orbits emerge. Furthermore, Figure 2 illustrates that, depending on the chosen value of parameter α_5, the population densities may converge to different steady state values. In this sense, since the dynamics do not depend exclusively on the initial conditions, we arbitrarily adopt the initial condition given in Eq (5.1) to study the joint influence of parameters α_5, ρ on the dynamics of the maximum value in steady state for each of the populations x_1, x_2, x_3, and x_4.

Algorithm 2. *Population maxima in steady state.*

1) *The parameters of system* (2.8) *assume the values of Table 2, except* ρ*, which is taken in* $(\rho_{c_1}, 1)$ *and* α_5*, which varies in* $(0, 9)$.
2) *The interval for each parameter is partitioned into 2000 equidistant points, and the cartesian product* $(0, 9) \times (\rho_{c_1}, 1)$ *is considered.*
3) *Integration time:* [0, 15000] *with step size* $\Delta t = 0.4$.
4) *System* (2.8) *is solved numerically with the initial conditions*

$$x_1(0) = 0.13957, \qquad x_2(0) = 0.70628 \qquad x_3(0) = 0.29975, \quad \textit{and} \quad x_4(0) = 0.04565. \tag{5.1}$$

and using the ODE45 integrator of Matlab with relative and absolute tolerances of 1×10^{-6}.
5) *Steady state: For each pair* (α_5, ρ)*, the initial condition* (5.1) *is taken, and the temporal evolution of each state variable is obtained. The last 3000 points of the temporal evolution are taken as steady state.*
6) *Maxima: For each pair* (α_5, ρ)*, the absolute maximum in the steady state of the temporal evolution for each state variable is obtained.*

Figure 7 is generated based on the implementation of Algorithm 2 to visualize the variability of $max(x_i)$ as a function of these parameters α_5 and ρ, facilitating the identification of different regions where significant changes are evident. The dynamics of the maximum in each population respond differently to variations in these parameters. For the pairs (α_5, ρ) that define region R13 (see Figure 3), which is characterized by the presence of stable periodic orbits, the tumor cell population x_2 reaches a maximum greater than 0.8, while the maximum of population x_1 remains below 0.3. Moreover, for the innate immune response x_3, the maximum reached is between 0.4 and 0.7, and in the adaptive immune response cell population x_4, the maximum is between 0.06 and 0.08. This scenario is unfavorable in tumor dynamics, as a high proportion of non-immunogenic tumor cells can enhance immune system evasion, promoting tumor progression and making its control and eventual elimination more difficult.

The dynamics observed in Figure 7(b) reveal regions where the concentrations of active immune response cells reach elevated levels at steady state, with x_3 approaching approximately 0.9. Such an intense activation may reflect scenarios of excessive immune stimulation, which, although initially favorable for tumor control, could compromise tissue integrity in the long term. Another unfavorable outcome is observed in region R4, where the tumor population x_1 reaches its maximum capacity (Figure 7(a)), leading to tumor progression and immune escape, since x_3 and x_4 become extinct in the steady state (Figure 7(b)). Conversely, in region R11, Figure 7(a) indicates a modest tumor burden; however, Figure 7(b) shows a significant increase in one of the immune cell populations. Based on Figure 7, it is possible to identify parameter configurations that minimize tumor burden while ensuring that the immune response population does not exceed a critical risk threshold. This threshold

may vary depending on the patient's condition and other factors associated with the type of cancer. For the purposes of our study and the analysis of the obtained results, as an illustrative example of the procedure for minimizing tumor burden, we set the threshold based on the dynamics shown in Figure 2, namely $x_3 < 0.45$ and $x_4 < 0.1$. This range is interpreted as a biologically relevant scenario in which the immune system effectively constrains tumor growth without triggering chronic inflammation or functional exhaustion of effector cells.

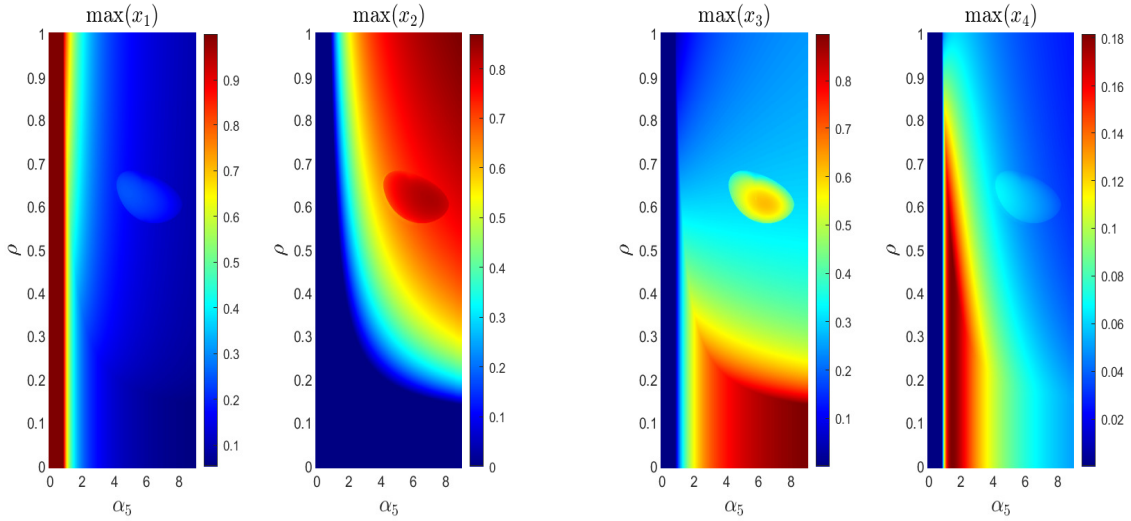

Figure 7. Dynamics of the maximum value in steady state with $\rho \in (\rho_{c_1}, 1)$, $\alpha_5 \in (0, 9)$, and the other parameters fixed at the values in Table 2. The color scales show the normalized density of each population in a steady state relative to the maximum value obtained from all possible combinations. a) Populations x_1 and x_2. b) Populations x_3 and x_4. This representation is obtained using Algorithm 2.

Based on the considered assumptions, the heat map proposed in Figure 7 indicates that, under nonzero initial conditions for all state variables, the most favorable scenario corresponds to the tumor latency state determined by the values of the parameters $\alpha_5 = 3.39494$ and $\rho = 0.40801$. The main criterion for defining this state as the most favorable is that the adaptive immune response x_4 remains below 0.1 and x_3 remains below 0.45. Additionally, within this set of solutions, a configuration is selected that minimizes the total tumor load $(x_1 + x_2)$ and the total immune response $(x_3 + x_4)$. Under these conditions, in the steady state, the trajectory converges to the equilibrium point given in Eq (5.2), which can be interpreted as a state in which the organism coexists with the disease without evidence of aggressive progression. At this point, the system maintains a dynamic balance in which the tumor neither disappears nor grows uncontrollably. This regime may represent a window of stability and long-term control in the course of the disease, establishing a biologically relevant scenario of tumor latency,

$$P_4 = [0.20495,\ 0.34116,\ 0.44634,\ 0.09993]\,. \tag{5.2}$$

5.2. Temporal evolutions and bifurcation diagram

Figure 8 presents examples of temporal evolutions that illustrate the dynamics characterized by the results discussed in previous sections. According to Table 3 and Figure 3, an asymptotic convergence to the equilibrium P_3 is reached in region R4. Figure 8(a) shows the tumor escape scenario where the population of immunogenic cancer cells x_1 grows until it reaches its maximum carrying capacity at steady state, while the innate immune cells x_3 and the adaptive immune cells x_4 approach values close to zero. This indicates a complete suppression of the immune response favoring tumor proliferation. In the dormant tumor scenario for immunogenic tumor (Figure 8(b)), the system converges to equilibrium P_3 with a FE structure. In this case, a high load of immune cells is able to contain the immunogenic tumor ($x_2 = 0$), keeping it in an immunological latency state that prevents uncontrolled growth, but without achieving its elimination. An example of tumor evolution in region R12 is presented in Figure 8(c), where convergence to the nontrivial equilibrium point P_4 given by (5.2) is observed. This represents the most favorable scenario according to the analysis conducted in Section 5.1.

On the other hand, in region R13, the system evolves toward a stable limit cycle. As shown in Figure 8(d), this dynamic is characterized by periodic oscillations in which tumor populations and immune cells fluctuate over time. This behavior results from the supercritical Hopf bifurcation discussed in section 4, implying that system (2.8) recurrently alternates between phases of tumor growth and reduction without reaching an equilibrium point. To analyze the dynamics of the periodic orbit in region R13, some bifurcation diagrams are constructed, and these are presented in Figure 9. Specifically, in Figure 9 (a) the parameters are set according to the values in Table 2, except for the two of interest: $\rho = 0.63$ and α_5, which varies within the interval $(0, 9)$. The results obtained confirm the dynamics shown in Figures 3 and 7. In particular, it validates the tumor escape scenario in region R4, the presence of a tumor in a latent state in R11 and R12, and the emergence of a one-periodic orbit in R13. No high period orbits or chaotic dynamics are identified within the parameter region R13.

In Figure 9(b), parameter $\alpha_5 = 5.8$, ρ is varied in the interval $(0, 1)$, and the other parameters are set to the values listed in Table 2. This diagram shows the transition between regions R11, R12, and R13. In R11 ($x_2 = 0$), while the immune response approaches a threshold of 0.8, the steady state population x_1 remains at a low level. In R12, the system converges to the nontrivial equilibrium point P_4, and in R13, a stable one-periodic orbit emerges. To construct the bifurcation diagrams of the Figure 9, we follow the methodology of the Algorithm 2 for the analysis of the steady state, but consider one of the parameters fixed, ρ or α_5, and the other as a bifurcation parameter divided into 500 equidistant points. The integration time, the numerical resolution, and the identification of the steady state defined in Algorithm 2 are used. From these data, the Poincaré section is constructed by calculating the maxima and minima of each variable in the steady state. Finally, a two dimensional plot of the bifurcation parameter versus the extreme values obtained is generated.

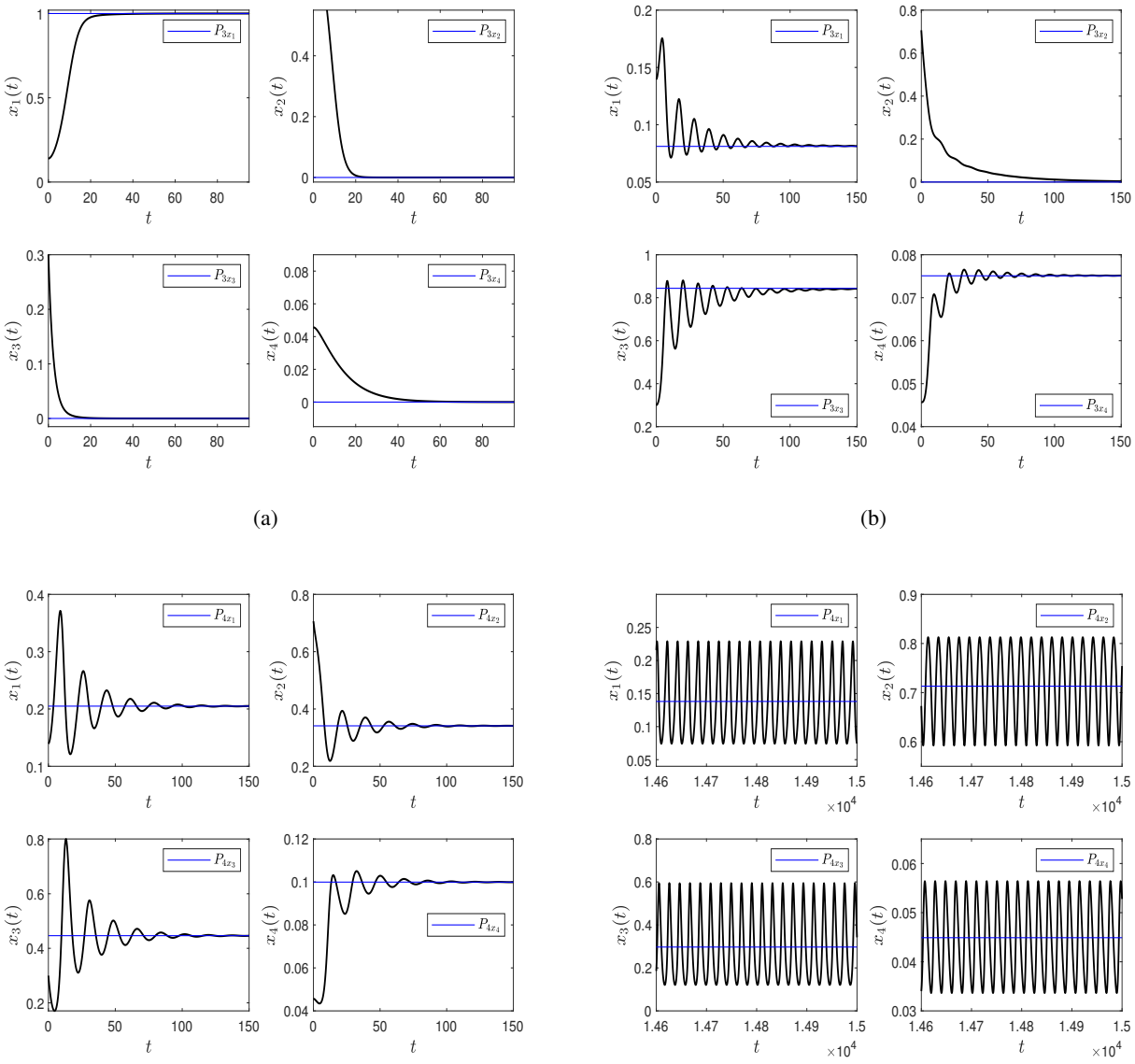

Figure 8. Temporal evolution of the state variables with the initial condition (5.1) and using the Matlab ODE45 integrator with relative and absolute tolerances of 1×10^{-6}. a) Tumor escape: Convergence to point P_3 in region R4, with $\rho = 0.63$ and $\alpha_5 = 0.5$. b) Latent immunogenic tumor: Convergence to P_3 in region R11 with $\rho = 0.15$ and $\alpha_5 = 6$. c) Tumor in a latent state:Convergence to the nontrivial equilibrium point P_4 in region R12, with $\rho = 0.40801$ and $\alpha_5 = 3.39494$. d) Immune regulation: Stable limit cycle with period one for $\rho = 0.63$ and $\alpha_5 = 6$, over region R13.

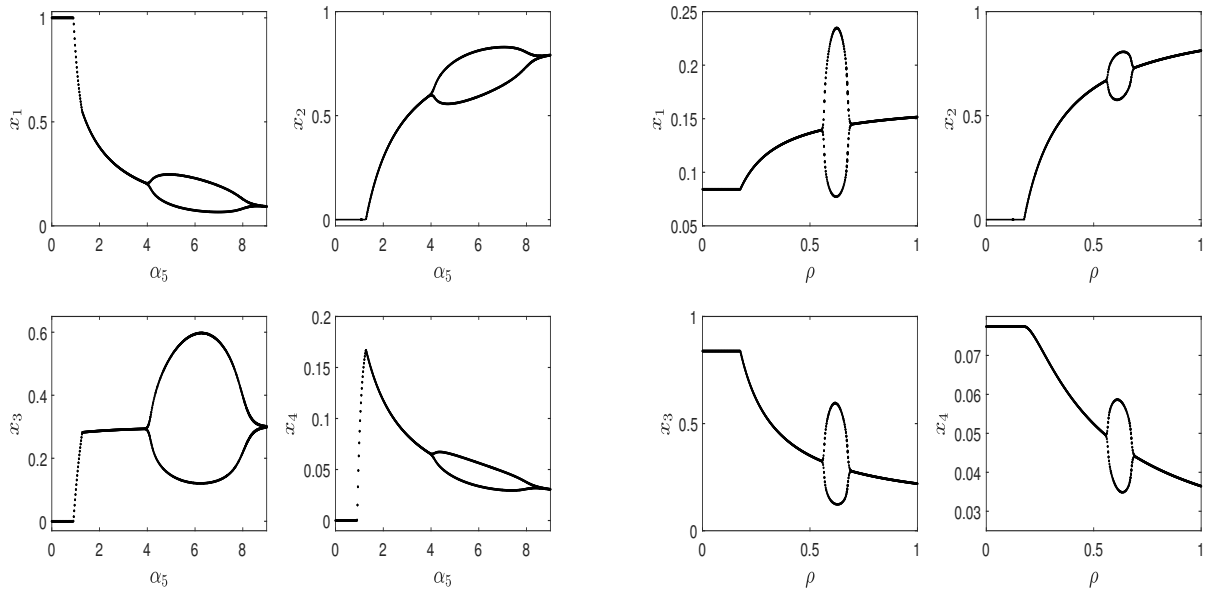

(a) (b)

Figure 9. Bifurcation diagrams. a) $\rho = 0.63$ and varying α_5. R4 for $\alpha_5 \in (0, \alpha_{5_c})$, R11 for $\alpha_5 \in (\alpha_{5_c}, 1.28)$, R12 for $\alpha_5 \in (1.28, 4.05) \cup \alpha_5 \in (8.34, 9)$, and R13 for $\alpha_5 \in (4.05, 8.34)$. b) $\alpha_5 = 5.8$ and varying ρ. R11 for $\rho \in (\rho_{c_1}, 0.18)$, R12 for $\alpha_5 \in (0.18, 0.55) \cup \alpha_5 \in (0.68, 1)$, and R13 for $\alpha_5 \in (0.55, 0.68)$. For the steady state analysis, we use the methodology of Algorithm 2. The bifurcation parameter is partitioned into 500 equidistant points; the integration time and integrator are similar to those in Algorithm 2. The other parameters in Table 2 must be taken into account as well.

6. Discussion and conclusions

In this article, we formulate mathematical model (2.8) to investigate the dynamics of primary cancerous tumors, considering two variants of malignant cells based on their level of immunogenicity, as well as the immune response in its two components, innate and adaptive. The system is expressed in terms of dimensionless combinations of parameters, which facilitates sensitivity analysis, since instead of varying many original parameters, the effect of a few effective parameters that encapsulate the dynamics can be studied. However, relating several original parameters may reduce traceability regarding which specific biological parameter is responsible for the observed variability. In this regard, the results presented in this work are based on a qualitative mathematical analysis under certain structural and parametric assumptions. These assumptions aim to highlight the fundamental dynamic mechanisms of the system but are not intended to encompass the full complexity of the oncological process or all biological variables involved in cancer.

The stability theory is applied to system (2.8), and all feasible equilibrium points within the region of interest are classified. In addition, a closed curve of supercritical Hopf bifurcation points is detected delineating the parameter region in which limit cycles emerge. Table 3 and Figure 3 provide a comprehensive summary of the local dynamics and define the robustness map of system (2.8). We

demonstrate how tumor progression and the coexistence of different cellular phenotypes are influenced by the proliferation rate of non-immunogenic cancer cells and the stimulation rate of the innate immune response, as well as promote the occurrence of bifurcations. By varying parameters α_5 and ρ defined in Eq (2.9), some of the immune editing scenarios defined in [24] are revealed, such as tumor escape in region R4, and in subsystem $x_1 = 0$ (see Figure 1). Additionally, the tumor latency scenario in R11 and R12 is observed, where convergence occurs to equilibrium P_3 ($x_2 = 0$) and to the nontrivial equilibrium point P_4, respectively. By applying Algorithm 1, a bi-parametric numerical continuation is constructed by varying ρ and α_5, resulting in the closed curve R10 (Figure 3). These results confirm that selecting a configuration of values (α_5, ρ) within region R13 and a non-trivial initial condition ensures that the trajectory of system (2.8) converges to a stable limit cycle, where all four interacting populations coexist. This finding aligns with previous observations in models of tumor heterogeneity and immune response [1, 17, 18, 25].

The identification of stability regions for non-immunogenic tumors in system (2.8) suggests that although these cellular phenotypes can evade the immune response, under certain conditions, an equilibrium is established within the tumor microenvironment. However, the immune response, while essential for host protection, can also generate collateral effects. In clinical cases, such as Covid-19, a phenomenon known as the cytokine storm has been observed, characterized by immune activation that surpasses a critical threshold and leads to severe tissue damage. The concept of an immunological threshold is useful for understanding the dual nature of the immune response, protective against infections or tumors, but it can be potentially lethal if it becomes excessive. Chen and Quach (2021) [26] argue that, in the cytokine storm syndrome, it is not merely immune activation that determines the clinical outcome, but the crossing of a critical activation threshold. According to Mangalmurti and Hunter (2020) [27], at this point, the immune response, initially protective, exceeds its regulatory function. This phenomenon also has direct implications for cancer development. Based on the characteristics of malignant cell progression, intense immune activation induced by therapies can trigger a clinically similar cytokine release syndrome, in which crossing an inflammatory threshold leads to severe patient toxicity [28]. Moreover, uncontrolled inflammation generates a microenvironment enriched with proinflammatory mediators that promote cell proliferation, angiogenesis, and the suppression of effective antitumor immune responses [29]. Thus, the same immunological mechanism that protects against infectious agents, once it exceeds its physiological threshold, can facilitate malignant transformation and tumor progression.

Based on the above, in this study, we consider $x_3 < 0.45$ and $x_4 < 0.1$ as indicative of a modest immune response, interpreting this range as a biologically relevant condition in which the immune system restrains tumor growth without inducing chronic inflammation or effector cell exhaustion. From this perspective, we find that the most favorable parameter configuration corresponds to $\alpha_5 = 3.39494$ and $\rho = 0.40801$, which generate the nontrivial equilibrium point FE given in Eq (5.2). Under these conditions, in the steady state, the immune response remains at a modest level, and the tumor burden is minimized. The analysis of system (2.8) was conducted within a dimensionless framework in order to simplify the mathematical formulation and highlight the qualitative mechanisms of the model. Consequently, comparison with experimental or clinical data requires restoring the original units of the variables and parameters, which involves performing the dimensionalization process again using Eqs (2.7) and (2.9). It is important to note that, for the interpretation of our results, we adopt certain assumptions regarding the state variables and

parameters in order to obtain a configuration that minimizes both tumor burden and immune response. Consequently, we invite the scientific community to interpret our findings with caution, viewing them primarily as a theoretical framework that provides insights into the dynamics than as direct quantitative predictions. The value of this analysis lies in the identification of plausible scenarios and the generation of hypotheses that may guide future experimental and clinical studies. In articles such as [2, 14], the importance of nonlinear dynamics in cancer treatment planning is emphasized. Owing to its nonlinear characteristics, model (2.8) may prove useful in designing immunotherapy strategies. By investigating the dynamics under the variation of other parameters, the model enables the identification of distinct dynamic regimes. This provides a foundation for future research, in which these regimes can be explored in greater depth and in relation to specific biological scenarios.

Use of AI tools declaration

The authors declare they have not used Artificial Intelligence (AI) tools in the creation of this article.

Acknowledgments

To Universidad Cooperativa de Colombia, Villavicencio-Colombia, for supporting the work of M.A. Nova Martínez. Also to Universidad del Tolima, Ibagué-Colombia, for supporting the work of H.A. Granada Díaz.

Conflict of interest

The authors declare there is no conflict of interest.

References

1. R. F. Alvarez, J. A. Barbuto, R. Venegeroles, A nonlinear mathematical model of cell-mediated immune response for tumor phenotypic heterogeneity, *J. Theor. Biol.*, **471** (2019), 42–50. https://doi.org/10.1016/j.jtbi.2019.03.025
2. E. Leschiera, T. Lorenzi, S. Shen, L. Almeida, C. Audebert, A mathematical model to study the impact of intra-tumour heterogeneity on anti-tumour CD8+ T cell immune response, *J. Theor. Biol.*, **538** (2022), 111028. https://doi.org/10.1016/j.jtbi.2022.111028
3. T. Singh, M. Bhattacharya, A. K. Mavi, A. Gulati, N. K. Sharma, S. Gaur, et al., Immunogenicity of cancer cells: An overview, *Cell. Signal.*, **113** (2024), 110952. ttps://doi.org/10.1016/j.cellsig.2023.110952
4. V. Debien, A. De Caluwé, X. Wang, M. Piccart-Gebhart, V. K. Tuohy, E. Romano, et al., Immunotherapy in breast cancer: An overview of current strategies and perspectives, *NPJ Breast Cancer*, **9** (2023), 1–10. https://doi.org/10.1038/s41523-023-00508-3
5. R. Rui, L. Zhou, S. He, Cancer immunotherapies: Advances and bottlenecks, *Front. Immunol.*, **14** (2023), 1212476. https://doi.org/10.3389/fimmu.2023.1212476

6. V. Shankaran, H. Ikeda, A. Bruce, J. White, P. Swanson, L. Old, et al., IFNγ and lymphocytes prevent primary tumour development and shape tumour immunogenicity, *Nature*, **410** (2001), 1107–1111. https://doi.org/10.1038/35074122
7. N. P. Restifo, M. J. Smyth, A. Snyder, Acquired resistance to immunotherapy and future challenges, *Nat. Rev. Cancer*, **16** (2016), 121-–126. https://doi.org/10.1038/nrc.2016.2
8. Y. Shu, J. Huang, Y. Dong, Y. Takeuchi, Mathematical modeling and bifurcation analysis of pro-and anti-tumor macrophages, *Appl. Math. Modell.*, **88** (2020), 758–773. https://doi.org/10.1016/j.apm.2020.06.042
9. A. S. Moffett, Y. Deng, H. Levine, Modeling the role of immune cell conversion in the tumor-immune microenvironment, *Bull. Math. Biol.*, **85** (2023), 85–93. https://doi.org/10.1007/s11538-023-01201-z
10. R. A. Flavell, S. Sanjabi, S. H. Wrzesinski, P. Licona-Limón, The polarization of immune cells in the tumour environment by TGFβ, *Nat. Rev. Immunol.*, **10** (2010), 554–567. https://doi.org/10.1038/nri2808
11. G. E. Mahlbacher, K. C. Reihmer, H. B. Frieboes, Mathematical modeling of tumor-immune cell interactions, *J. Theor. Biol.*, **469** (2019), 47–60. https://doi.org/10.1016/j.jtbi.2019.03.002
12. K. P. Wilkie, P. Hahnfeldt, Modeling the dichotomy of the immune response to cancer: Cytotoxic effects and tumor-promoting inflammation, *Bull. Math. Biol.*, **79** (2017), 1426–1448. https://doi.org/10.1007/s11538-017-0291-4
13. J. Li, X. Xie, Y. Chen, D. Zhang, Complex dynamics of a tumor-immune system with antigenicity, *Appl. Math. Comput.*, **400** (2021), 126052. https://doi.org/10.1016/j.amc.2021.126052
14. M. Ghanizadeh, S. P. Shariatpanahi, B. Goliaei, C. Rüegg, Mathematical modeling approach of cancer immunoediting reveals new insights in targeted-therapy and timing plan of cancer treatment, *Chaos Solitons Fractals*, **152** (2021), 111349. https://doi.org/10.1016/j.chaos.2021.111349
15. O. Nave, M. Sigron, A mathematical model for cancer treatment based on combination of anti-angiogenic and immune cell therapies, *Results Appl. Math.*, **16** (2022), 100330. https://doi.org/10.1016/j.rinam.2022.100330
16. V. Kuznetsov, I. Makalkin, M. Taylor, A. Perelson, Nonlinear dynamics of immunogenic tumors: Parameter estimation and global bifurcation analysis, *Bull. Math. Biol.*, **56** (1994), 295–321. https://doi.org/10.1016/S0092-8240(05)80260-5
17. L. G. De Pillis, A. Radunskaya, A mathematical tumor model with immune resistance and drug therapy: An optimal control approach, *Comput. Math. Methods Med.*, **3** (2001), 79–100. https://doi.org/10.1080/10273660108833067
18. M. Itik, S. P. Banks, Chaos in a three-dimensional cancer model, *Int. J. Bifurcation Chaos*, **20** (2010), 71–79. https://doi.org/10.1142/S0218127410025417
19. A. N. Kanatnikov, K. E. Starkov, Ultimate dynamics of the Two-Phenotype cancer model: Attracting sets and global cancer eradication conditions, *Mathematics*, **11** (2023), 4275. https://doi.org/10.3390/math11204275

20. L. Perko, *Differential Equations and Dynamical Systems*, 3rd edition, Springer New York, 2001. https://doi.org/10.1007/978-1-4613-0003-8

21. W. Govaerts, Y. Kuznetsov, H. Meijer, Matcont: Numerical bifurcation analysis toolbox in Matlab, 2025. Available: https://sourceforge.net/projects/matcont/.

22. Y. A. Kuznetsov, *Elements of Applied Bifurcation Theory*, 4th edition, Springer Cham, New York, 2023. https://doi.org/10.1007/978-3-031-22007-4

23. J. Guckenheimer, P. Holmes, *Nonlinear Oscillations Dynamical Systems, and Bifurcations of Vector Fields*, 2nd edition,Springer New York, 1983. https://doi.org/10.1007/978-1-4612-1140-2

24. G. P. Dunn, L. J. Old, R. D. Schreiber, The three Es of cancer immunoediting, *Ann. Rev. Immunol.*, **22** (2004), 329–360. https://doi.org/10.1146/annurev.immunol.22.012703.104803

25. M. A. N. Martínez, H. A. G. Díaz, P. E. Calderón Saavedra, Dynamics of a mathematical model of cancer and immunoediting scenarios under the variation of the immune cell activation rate, *Int. J. Bifurcation Chaos*, **32** (2022), 2230014. https://doi.org/10.1142/S0218127422300142

26. L. Chen, T. Quach, COVID-19 cytokine storm syndrome: A threshold concept, *Lancet Microbe*, **2** (2021), 49–50. https://doi.org/10.1016/S2666-5247(20)30223-8

27. N. Mangalmurti, C. A. Hunter, Cytokine storms: Understanding COVID-19, *Immunity*, **53** (2020), 19–25. https://doi.org/10.1016/j.immuni.2020.06.017

28. J. S. Marshall, R. Warrington, W. Watson, H. L. Kim, An introduction to immunology and immunopathology, *Allergy Asthma, Clin. Immunol.*, **14** (2018), 4275. https://doi.org/10.1186/s13223-018-0278-1

29. R. Q. Cron, G. Goyal, W. W. Chatham, Cytokine storm syndrome, *Ann. Rev. Med.*, **74** (2023), 321–337. https://doi.org/10.1146/annurev-med-042921-112837

AIMS Press